

Short Communication

Improved Surface Properties for Nanotube Growth on Selective Laser Melted Porous Ti6Al4V Alloy via Chemical Etching

Xiaoqing Ni, Liang Zhang*, Wenheng Wu, Jia Song, Beibei He, Dexiang Zhu

Shanghai Engineering Research Center of 3D Printing Materials, Shanghai Research Institute of Materials, Shanghai 200437, China

*E-mail: liangustb@126.com

Received: 25 January 2019 / Accepted: 5 March 2019 / Published: 10 May 2019

In this work, porous Ti6Al4V components with a 400 μm interval were prepared by selective laser melting (SLM), one of most popular powder-bed additive manufacturing technologies for metallic alloys, there were many un-melted powders adhered to the as-received substrate framework. To improve the bio-functional property, surface treatment for this complex structure must be taken into consideration and chemical etching for proper time can remove the trapped powders. Anodic oxidation experiments showed that non-uniform nanotubes grew on the trapped powders, while nanotubes grew uniformly on the chemical etched substrate and the diameter of nanotubes was about 100 nm all over the place. The electrochemical experiments and cell proliferation results all showed that the chemical etching method can improve the corrosion resistance and biocompatibility of the SLM porous Ti6Al4V.

Keywords: Ti-6Al-4V; Selective laser melting; Nanotube; Porous materials; Chemical etching

1. INTRODUCTION

Biomedical implants are extensively required to repair, replace, or modify diseased or damaged parts of the musculoskeletal system and need to be manufactured from materials that are biocompatible and stable during the service time [1-2], and the implanted alloys are generally fabricated from stainless steels, Co/Cr-based alloys, titanium and its alloys [3-10]. However, implant failures often occur, where 42% of failures are due to fracture, 24% caused by corrosion, and 14% a result of a vicious organization along with the implants [11]. The elastic modulus of the titanium alloys is low compared with steels but is high relative to bone tissue [12-13] and this mismatch reduces the stress transferred to the adjoining bone that can result in undesirable bone resorption. As in this case, two methods have been considered: the development of new titanium alloys with lower elastic modulus [14] and the fabrication of porous titanium parts that can reduce the effective elastic modulus, or the stiffness [15-16]. The latter has the

advantage of allowing the bone to grow inside the implant, thus enhancing implant fixation. Currently, selective laser melting (SLM), which is a three-dimensional printing processing, that can produce complex and precise porous parts combining with computer CAD system. Meanwhile, SLM has other significant advantages, including a reduction in the number of required post-processing steps, control of the composition and microstructure by printing multiple materials with optimized printing parameters [17-19]. At present, AlSi10Mg, TiAl6V4, and CoCr alloys, can be reliably printed [20-22], and the Fe-based and Ni-based alloys were fabricated by SLM recently [23-24]. During the AM process, the local rapid heating and fast cooling rates coupled with thermal cycling induces the formation of unique microstructures with refined grain structures, dislocation cell substructures, and internal residual stresses. They also cause the formation of metallurgical defects, including micro-cracks, entrapped gas pore, dendritic growth along the building direction, and the roughness [25]. However, surface modification of 3D printed porous metals is more challenging than that of solid implant due to the complex three-dimensional structure, one of intricate issues is that the powder trapped within the porous structure mesh during the fabrication process and they are hard to be removed [26-27]. Thus, corrosion must be considered with regard to its service life in the future after the wide application of AM technology for practical life and production [28-34].

Generally, surface condition plays an important role on the corrosion properties of materials, and pitting susceptibility [35-38] and general corrosion rate [39-41] all increased with the increase in the surface roughness of materials. Meanwhile, surface condition was a big problem for additive manufacturing, especially for anti-corrosion property involving the interfacial reaction, the surface roughness of the parts fabricated by SLM is usually higher than manufactured by methods such as milling [42]. For this reason, post-processing such as sandblasting or chemical etching are usually implemented [43], however, the sandblasting was not unpractical for the porous structure and the chemical etching might show some potential. Ti and Ti alloys are of utmost interest with regard to the additive manufacturing field, and Ti combines broad industrial application in high performance parts with high machining costs, hard molding and long lead time in conventional processing [44-45]. Among titanium alloys, Ti6Al4V is the most widely used material for many engineering parts and biomedical implants. Actually, tensile ductility was doubled after surface modification of the SLM-fabricated Ti-6Al-4V by chemical etching [46].

Within the scope of this project, a chemical etching process was evaluated for sintered powder removal and the follow-up anodic oxidization was conducted for the first time to evaluate the effect after treatment. Electrochemical experiments and cell proliferation tests were carried out to compare the corrosion resistance and biocompatibility. The results are expected to contribute valuable information for developing SLM porous titanium alloys for future implant applications.

2. MATERIALS AND METHODS

2.1. Sample preparation

The chemical compositions of the powder used for SLM-produced Ti-6Al-4V were similar with the commercial wrought (wt. %): Al 6.31, V 4.03, Fe 0.25, N 0.03, O 0.15, C 0.02 and Ti balance. Figure

1 (a) showed the size distribution of the gas-atomized powder and the morphology of the powder particles, the diameter ranged from 10 to 50 μm with an average of around 34 μm .

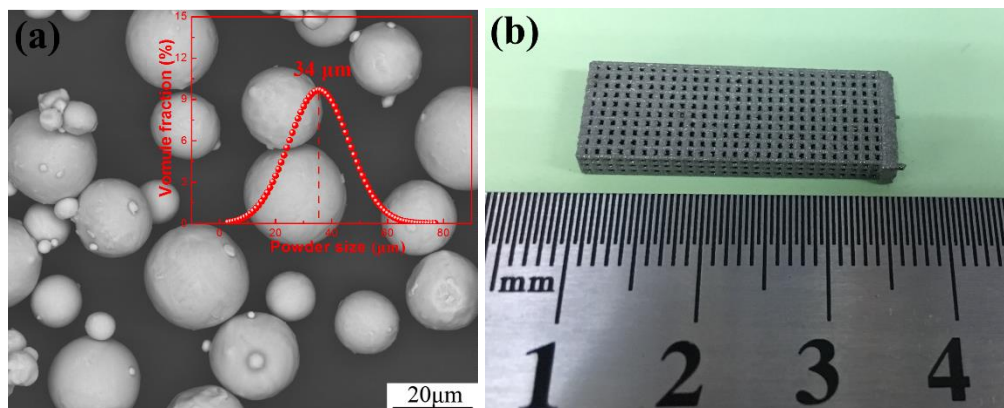


Figure 1. (a) The gas-atomized powder size distribution and the morphology of the powders, and (b) an image of a SLM porous Ti-6Al-4V sample.

Samples were fabricated using SLM with an EOS M280 system (Germany), as shown in Figure 1(b), which was equipped with a 400W Yb:YAG fibre laser (wavelength of 1070 nm), operated at a scan speed of 1200 mm/s and a spot size of 80 μm . The SLM porous samples were produced in continuous laser mode (250 W) and the hatch spacing (distance between scan lines) and the layer thickness were all about 25 μm .

2.2 Surface treatment

The specimens were etched in Kroll reagent (3 mL 40 vol. % HF, 6 mL 70 vol. % HNO₃ and 100 mL water) at room temperature for 5 min and 15 min, respectively. As a contrast, a SLM specimen was ultrasonically cleaned in ethanol for 2 hours at 30 Hz to figure out whether the trapped powders can be shaken off. Then, all specimens were cleaned in ethanol and distilled water, followed by drying in cool air.

2.3. Preparation of nanotubes

Nanotubes were prepared by an anodization process, which was performed using a two-electrode system. The SLM Ti-6Al-4V parts acted as the anode, while the Pt circle was used as the cathode, and the distance between the anode and the cathode was maintained at 4 cm. The schematic diagram of anodic oxidation device was displayed in Figure 2 and the Pt circle here was to make sure the nanotubes grow uniformly in different directions on the porous structure. The anode and the cathode were submerged into an electrolyte solution (0.36 M NH₄F + 80 vol. % glycerol + 20 vol. % distilled water) at 20 V supplied by DC power (RXN-3030D, BOSHIWANG Power, China) for 3 h. Next, the as-formed samples were cleaned in ethanol and distilled water, followed by drying in cool air. The surface morphologies were identified by FE-SEM (Quanta 450, FEI, USA).

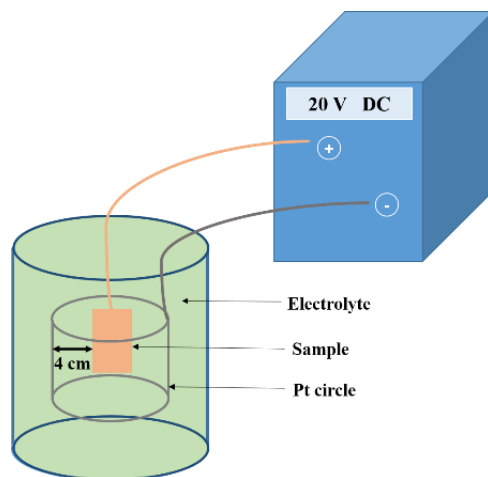


Figure 2. Schematic diagram of anodic oxidation device

2.4. Electrochemical and biological compatibility experiments

Potentiodynamic polarisation was conducted using a Princeton VersaStudio 3F electrochemical workstation in a conventional 3-electrode cell with a saturated calomel electrode (SCE) and platinum foil as the reference and counter electrodes, respectively. All samples were mounted in a plastic tube and sealed with epoxy resin with exposure of the side view to the outside. Potentiodynamic polarisation was initiated from a potential 250 mV lower than the open-circuit potential at a scanning rate of 0.1667 mV/s. All reported potentials in this work were relative to SCE and the electrochemical measurements were carried out in the SBF solution at 37 ± 0.2 °C.

All samples were sterilized by soaking in 75% ethanol for 30 min, followed by a 30 min UV exposure on both sides of the Ti6Al4V samples. After immersing the samples in the complete medium for 4 h, it was collected, mixed with the cell count kit-8 (CCK-8) mother liquor, and left for 2 h at 37 °C. Then, 1 mL of cell suspension containing 2×10^5 cells was seeded and the CCK-8 assay (Dojindo Molecular Technology) was used to quantitatively evaluate the cell proliferation after culturing for 1, 3, and 7 days. The tests for each sample were performed at least three times for data reproducibility.

3. RESULTS AND DISCUSSION

Figure 3 displayed the surface morphology of the SLM porous Ti-6Al-4V: (a)(b) as received; (c)(d) ultrasonic treatment in ethanol for 2h; (e)(f) chemical etching for 5 min; (g)(h) chemical etching for 15 min. Pores greater than 200 μm usually allow the migration of osteoprogenitor cells into the scaffolds and lower the overall scaffold density [47]. Frosch [48] further established that the optimum channel diameter for the formation of bone tissue was 300 ~ 400 μm and the distance between the laser scanning lines in our work was set as 400 μm . Meanwhile, we can see on the top surface that there were many un-melted powders adhered to the as received substrate in Figure 3 (b), and ultrasonic treatment for 2 hours did not work here as we can see in Figure 3 (d). However, chemical etching for proper time

can remove the trapped powders as displayed in Figure 3 (f) but further etching for 15 minutes will destroy the matrix in Figure 3 (g) and (h).

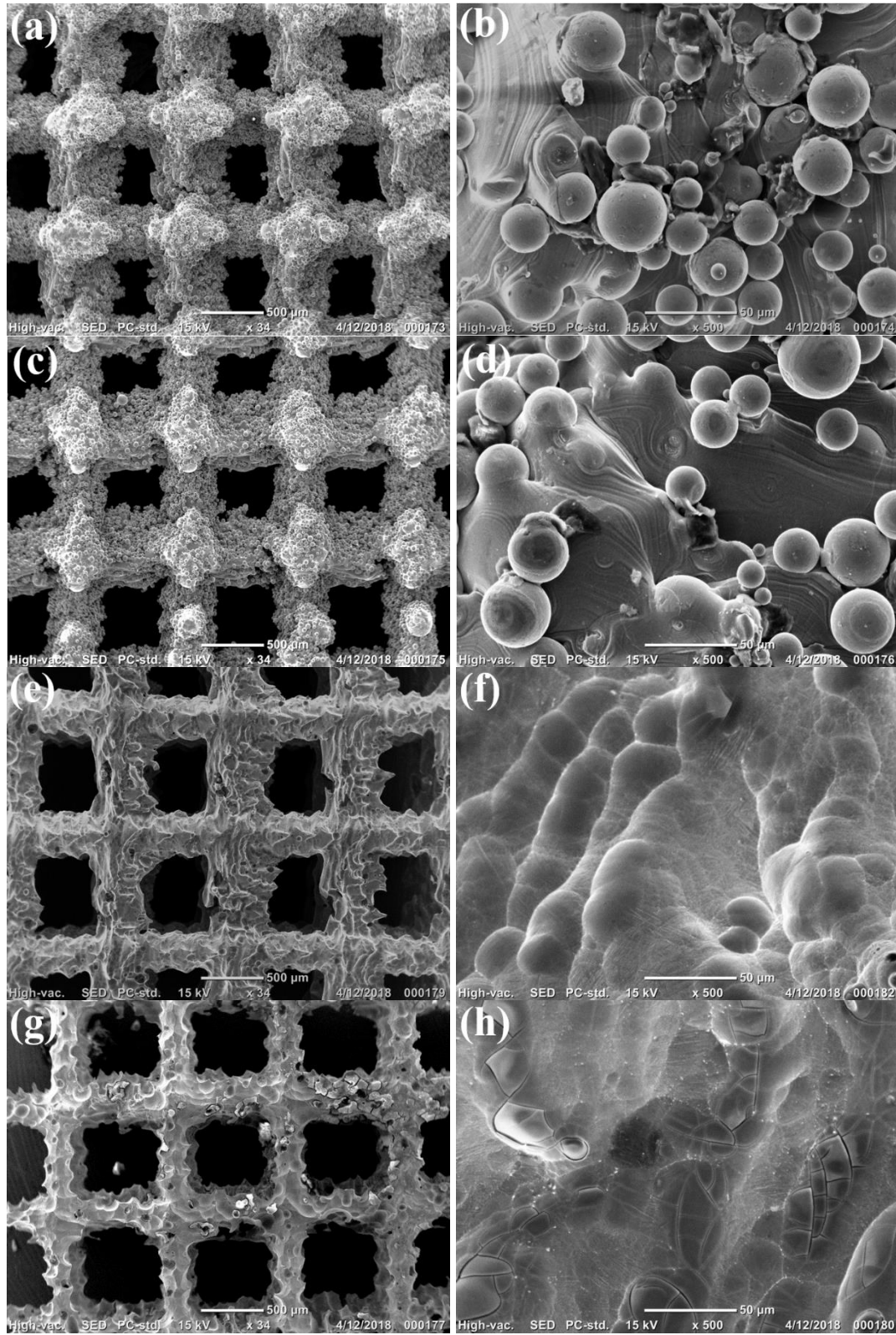


Figure 3. Surface morphology of the SLM porous Ti-6Al-4V: (a)(b) as received; (c)(d) ultrasonic treatment in ethanol for 2h; (e)(f) chemical etching for 5 min; (g)(h) chemical etching for 15 min.

To further observe the internal morphology of the porous structure, the cross sectional samples were prepared and shown in Figure 4. Similarly, the internal powder can not be shaken off either as displayed in Figure 4 (b), while the powder was totally etched after 5 minutes immersion, and the internal frame structure was destroyed and became thinner after longer etching. Thus we can conclude that the powder adhered to the whole porous structure can be etched well for proper time in Kroll reagent.

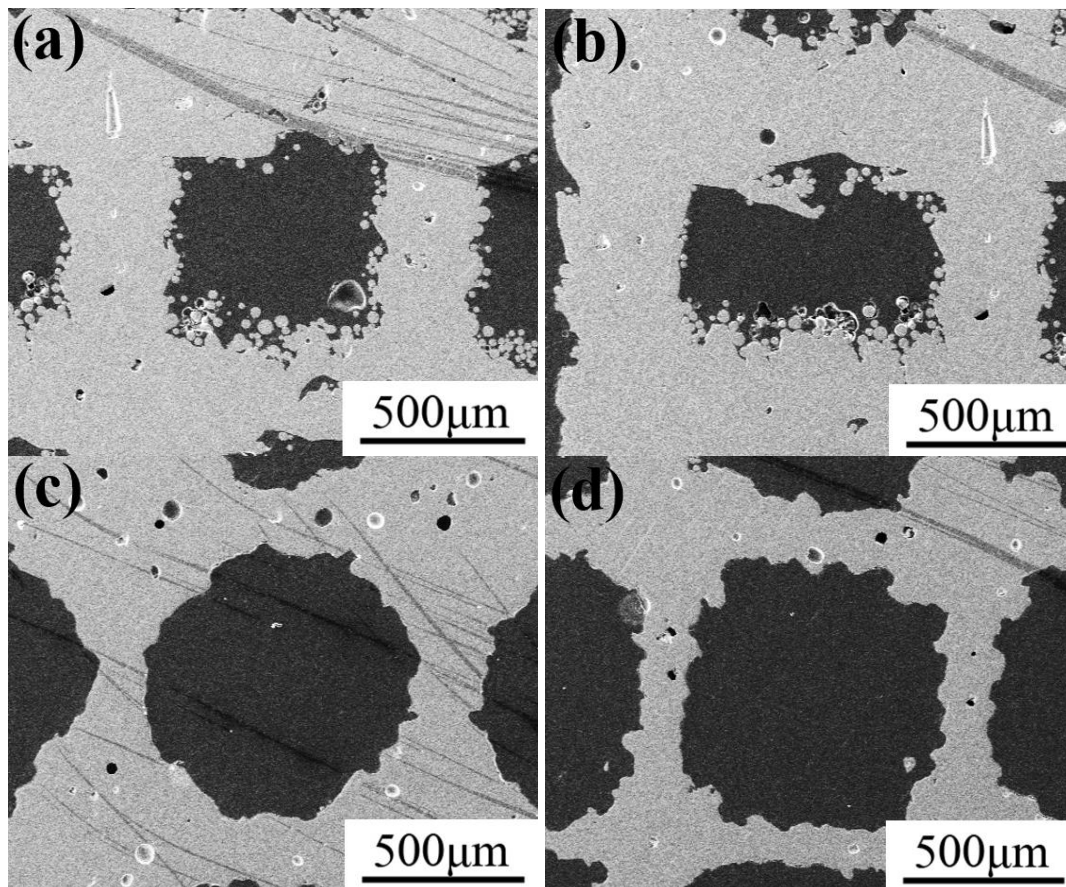
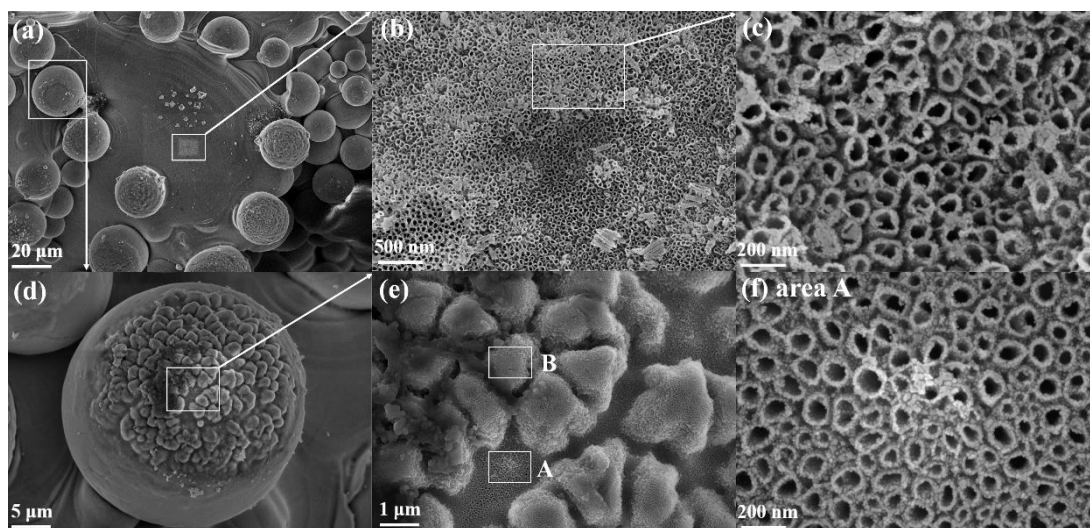


Figure 4. Internal cross section morphology of the SLM porous Ti-6Al-4V: (a) as received, (b) ultrasonic treatment in ethanol for 2h, (c) chemical etching for 5 min and (d) chemical etching for 15 min.



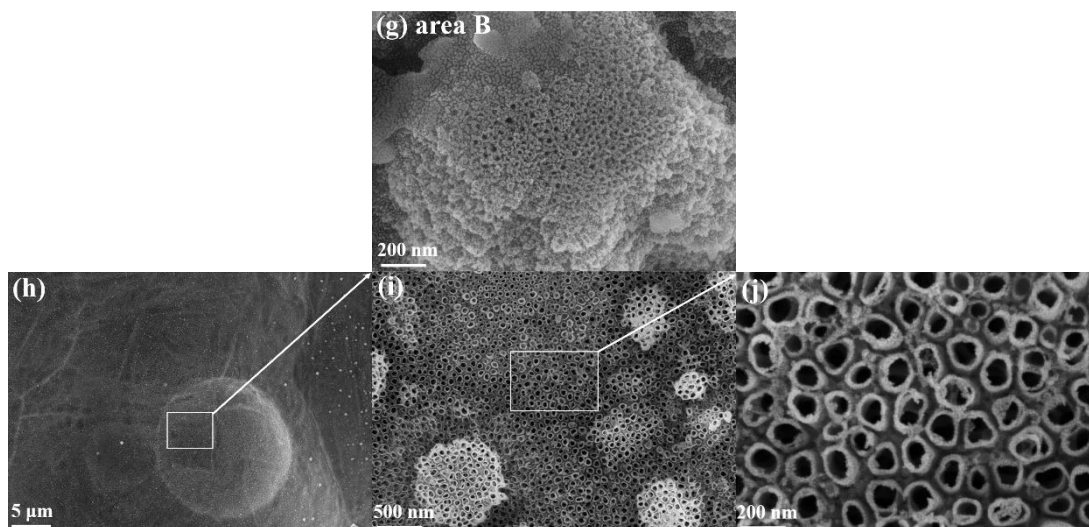


Figure 5. Surface morphology after anodic oxidation treatment: (a)~(g) as received SLM porous Ti-6Al-4V; (h)~(f) SLM porous Ti-6Al-4V after chemical etching for 5 min.

Figure 5 showed the surface morphology after oxidation treatment, we can see that the trapped powders can also be oxidized but there were inhomogeneous nanotubes in the further enlarged Figure 5 (f) and (g). At the top of the powders (mark B), the average diameter of the nanotubes was relative small (around 20 nm), while the diameter was about 80 nm at area A, those differences can be attributed to the non-uniform element distribution or structure in the un-melted Ti6Al4V powders [49]. For the chemical etched substrate, the nanotubes grew uniformly and the diameter was about 100 nm all over the place, thus indicating the removal of the trapped power was very essential before anodic oxidation. Meanwhile, this nanometer scale tube was very suitable for cell adhesion, proliferation and differentiation [50].

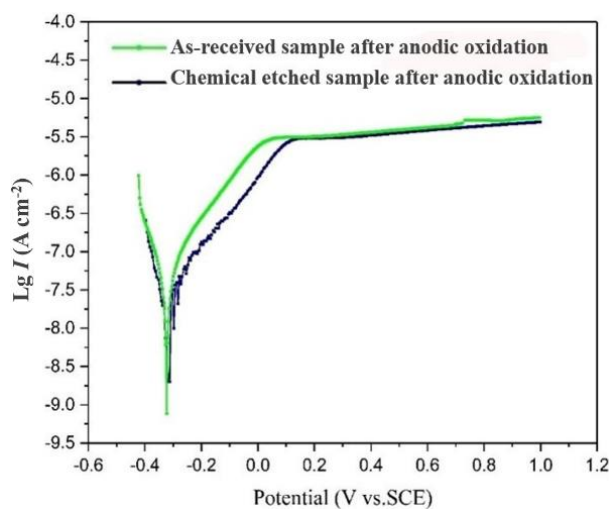


Figure 6. Potentiodynamic polarisation of the as-received SLM porous Ti-6Al-4V and chemical etched SLM porous Ti-6Al-4V after anodic oxidation in SBF (37 ± 0.2 °C). Scanning rate = 0.1667 mV/s.

Figure 6 displayed the potentiodynamic polarisation results of the as-received SLM porous Ti-6Al-4V and chemical etched SLM porous Ti-6Al-4V after anodic oxidation in SBF (37 ± 0.2 °C) and we can see the corrosion potential did not change after chemical etching and was around $-0.32 V_{SCE}$.

However, the anodic polarization current density for the chemical etched sample was smaller than that of the as-received one, which indicated a better corrosion resistance for the SLM Ti6Al4V after the removal of the trapped powders [51-53]. Meanwhile, the trapped powders might fall off during the service, which might also lead to the poor durability.

To further evaluate the biocompatibility, Figure 7 (a) displayed the result of cell viability test of MC3T3-E1 cultured on three different surfaces for 1 day, 3 days and 7 days respectively. The data of each group were obtained through six repeated experiments. CCK-8 staining is directly proportional to the number of living cells. Therefore, the higher the absorbance is, the higher the surface cell activity is. From Figure 7-8a, it can be seen that chemical etched porous Ti6Al4V after anodic oxidation has higher cell activity and has a long-term promoting effect on cell proliferation. Alkaline phosphatase (ALP) expression is associated with osteoblast differentiation, so the activity of ALP is an important parameter to characterize the material surface promoting osteoblast differentiation and surface biocompatibility [54]. From Figure 7 (b), it can be seen that the surface of chemical etched porous Ti6Al4V after anodic oxidation has the highest ALP activity of osteoblasts compared with the surface of other two samples, that is, the surface of chemical etched porous Ti6Al4V has the most obvious promoting effect on the differentiation of osteoblasts, which enhances the adhesion, proliferation and differentiation ability of osteoblasts [55]. Meanwhile, powder may fall off during service and cause inflammation, and in this work, we can see that appropriate chemical etching method can achieve admirable results. More systematic works about the chemical etching technique should be conducted in the near future with the increasing variety of AM materials.

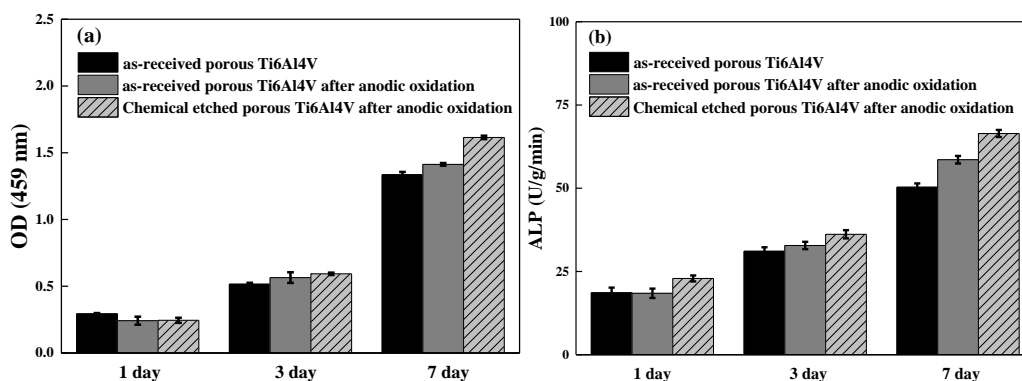


Figure 7. The cell proliferation and alkaline phosphatase activities on different surfaces after incubation for 1, 3 and 7 days by the CCK-8 assay.

4. CONCLUSIONS

This study compared the nanotube growth on as-received and chemical etched SLM porous Ti6Al4V for the first time, the findings led to the following conclusions: Many un-melted powders adhered to the as received SLM porous Ti6Al4V substrate, and chemical etching for proper time can remove the trapped powders. Non-uniform nanotubes grew on the trapped powders, while nanotubes grew uniformly on the chemical etched substrate, leading to an improved corrosion resistance. The cell

proliferation and alkaline phosphatase activities results showed that the chemical etching method can improve the surface biocompatibility of the SLM porous Ti6Al4V, which contributed to the further application of the AM biomaterials.

ACKNOWLEDGMENTS

This work was supported by Technology Innovation Project (Project Number 18SG-07), Natural Science Foundation of Shanghai (Project Number 17ZR1409200), Shanghai Rising-Star Program (Project Number 18QB1400600), Shanghai Sailing Program (Project Number 17YF1405400), the project to strengthen industrial development at the grass-roots level (Project Number TC160A310/19) and Young science and technology talents upgrading scheme (18SG-15). The authors also appreciate the work by Dr. Decheng Kong and Prof. Chaofang Dong from the University of Science and technology in Beijing.

References

1. S. J. Hollister, *Nat. Mater.*, 4 (2005) 518.
2. H. K. Koh, J. J. Piotrowski, S. Kumanyika and J. E. Fielding, *Health Educ. Behav.*, 38 (2011) 551.
3. A. Ramarolahy, P. Castany, F. Prima, P. Laheurte, I. Peron and T. Gloriant, *J. Mech. Behav. Biomed.*, 9 (2012) 83.
4. P. Laheurte, F. Prima, A. Eberhardt, T. Gloriant, M. Wary and E. Patoor, *J. Mech. Behav. Biomed.*, 3 (2010) 565.
5. S. M. Hosseinalipour, A. Ershad-Langroudi, A. N. Hayati and A. M. Nabizade-Haghighi, *Prog. Org. Coat.*, 67 (2010) 371.
6. J. L. Chen, C. Chen, Z. Y. Chen, J. Y. Chen, Q. L. Li and N. Huang, *J. Biomed. Mater. Res. A*, 95 (2010) 341.
7. I. T. Meredith, S. Verheye, C. L. Dubois, J. Dens, J. Fajadet, D. Carrie, S. Walsh, K. G. Oldroyd, O. Varenne, S. El-Jack, R. Moreno, A. A. Joshi, D. J. Allocco and K. D. Dawkins, *J. Am. Coll. Cardiol.*, 59 (2012) 1362.
8. D. Kong, X. Ni, C. Dong, X. Lei, L. Zhang, C. Man, J. Yao, X. Cheng and X. Li, *Mater. Design*, 152 (2018) 88.
9. D. Kong, X. Ni, C. Dong, L. Zhang, C. Man, X. Cheng and X. Li, *Mater. Lett.*, 235 (2019) 1.
10. C. Man, C. Dong, T. Liu, D. Kong, D. Wang and X. Li, *Appl. Surf. Sci.*, 467 (2019) 193.
11. I. Sailer, A. Philipp, A. Zembic, B. E. Pjetursson, C. H. F. Hammerle and M. Zwahlen, *Clin. Oral. Implan. Res.*, 20 (2009) 4.
12. R. H. Jin and M. Long, *Biomaterials*, 19 (1998) 1621.
13. X. Liu, P. Chu and C. Ding, *Mater. Sci. Eng. R: Rep.*, 47 (2004) 49.
14. M. Niinomi, *J. Mech. Behav. Biomed. Mater.*, 1 (2008) 30.
15. Y. J. Liu, S. J. Li, H. L. Wang, W. T. Hou, Y. L. Hao, R. Yang, T. B. Sercombe and L. C. Zhang, *Acta Mater.*, 113 (2016) 56.
16. M. Zhou, P. Xiong, Z. Jia, J. Tan, Y. Cheng, X. Liu, H. Cai and Y. Zheng, *Mater. Lett.*, 202 (2017) 9.
17. C. Y. Yap, C. K. Chua, Z. L. Dong, Z. H. Liu, D. Q. Zhang, L. E. Loh and S. L. Sing, *Appl. Phys. Rev.*, 2 (2015) 101.
18. X. Ni, D. Kong, W. Wu, L. Zhang, C. Dong, B. He, L. Lu, K. Wu and D. Zhu, *J. Mater. Eng. Perform.*, 27 (2018) 3667.
19. D. Kong, X. Ni, C. Dong, L. Zhang, C. Man, J. Yao, K. Xiao and X. Li, *Electrochim. Acta*, 276 (2018) 293.

20. J. J. Lewandowski and M. Seifi, *Annu. Rev. Mater. Res.*, 46 (2016) 151.
21. W. E. Frazier, *J. Mater. Eng. Perform.*, 23 (2014) 1917.
22. A. Townsend, N. Senin, L. Blunt, R. K. Leach and J. S. Taylor, *Precis. Eng.*, 46 (2016) 34.
23. S. Gorsse, C. Hutchinson, M. Goune and R. Banerjee, *Sci. Technol. Adv. Mater.*, 18 (2017) 584.
24. D. Kong, C. Dong, X. Ni, L. Zhang, C. Man, J. Yao, Y. Ji, Y. Ying, K. Xiao, X. Cheng and X. Li, *J. Alloy. Compd.*, 785 (2019) 826.
25. G. Sander, J. Tan, P. Balan, O. Gharbi, D. R. Feenstra, L. Singer, S. Thomas, R. G. Kelly, J. R. Scully and N. Birbilis, *Corrosion*, 74 (2018) 1318.
26. X. Zhao, S. Li, M. Zhang, Y. Liu, T. B. Sercombe, S. Wang, Y. Hao, R. Yang and L. E. Murr, *Mater. Design*, 95 (2016) 21.
27. S. Y. Chen, J. C. Huang, C. T. Pan, C. H. Lin, T. L. Yang, Y. S. Huang, C. H. Ou, L. Y. Chen, D. Y. Lin, H. K. Lin, T. H. Li, J. S. C. Jang and C. C. Yang, *J. Alloy. Compd.*, 713 (2017) 248.
28. C. F. Dong, F. X. Mao, S. J. Gao, S. Sharifi-Asl, P. Lu and D. D. Macdonald, *J. Electrochem. Soc.*, 163 (2016) C707.
29. S. J. Gao, C. F. Dong, H. Luo, K. Xiao, X. M. Pan and X. G. Li, *Electrochim. Acta*, 114 (2013) 233.
30. H. Luo, C. F. Dong, K. Xiao and X. G. Li, *Appl. Surf. Sci.*, 258 (2011) 631.
31. Y. B. Hu, C. F. Dong, M. Sun, K. Xiao, P. Zhong and X. G. Li, *Corros. Sci.*, 53 (2011) 4159.
32. C. F. Dong, Z. Y. Liu, X. G. Li and Y. F. Cheng, *Int. J. Hydrogen Energ.*, 34 (2009) 9879.
33. C. F. Dong, X. G. Li, Z. Y. Liu and Y. R. Zhang, *J. Alloy. Compd.*, 484 (2009) 966.
34. C. F. Dong, A. Q. Fu, X. G. Li and Y. F. Cheng, *Electrochim. Acta*, 54 (2008) 628.
35. Y. Zuo, H. T. Wang and J. P. Xiong, *Corros. Sci.*, 44 (2002) 25.
36. D. C. Kong, A. N. Xu, C. F. Dong, F. X. Mao, K. Xiao, X. G. Li and D. D. Macdonald, *Corros. Sci.*, 116 (2017) 34.
37. D. Kong, C. Dong, X. Wei, C. Man, X. Lei, F. Mao and X. Li, *Electrochim. Acta*, 292 (2018) 817.
38. D. Kong, C. Dong, X. Ni, C. Man, K. Xiao and X. Li, *Appl. Surf. Sci.*, 455 (2018) 543.
39. A. Shahryari, W. Kamal and S. Omanovic, *Mater. Lett.*, 62 (2008) 3906.
40. D. C. Kong, C. F. Dong, A. N. Xu, C. He and X. G. Li, *Corros. Eng. Sci. Techn.*, 52 (2017) 188.
41. D. Kong, C. Dong, Z. Zheng, F. Mao, A. Xu, X. Ni, C. Man, J. Yao, K. Xiao and X. Li, *Appl. Surf. Sci.*, 440 (2018) 245.
42. D. Wang, Y. Liu, Y. Yang and D. Xiao, *Rapid Prototyping J.*, 22 (2016) 706.
43. D. K. Pattanayak, A. Fukuda, T. Matsushita, M. Takemoto, S. Fujibayashi, K. Sasaki, N. Nishida, T. Nakamura and T. Kokubo, *Acta Biomater.*, 7 (2011) 1398.
44. Y. S. Hedberg, B. Qian, Z. J. Shen, S. Virtanen and I. O. Wallinder, *Dent. Mater.*, 30 (2014) 525.
45. H. R. Kim, Y. K. Kim, J. S. Son, B. K. Min, K. H. Kim and T. Y. Kwon, *Mater. Lett.*, 178 (2016) 300.
46. Y. Y. Sun, S. Gulizia, C. H. Oh, D. Fraser, M. Leary, Y. F. Yang and M. Qian, *Jom* 68 (2016) 791.
47. H. Zreiqat, S. M. Valenzuela, B. Ben Nissan, R. Roest, C. Knabe, R. J. Radlanski, H. Renz and P. J. Evans, *Biomaterials*, 26 (2005) 7579.
48. K. H. Frosch, F. Barvencik, V. Viereck, C. H. Lohmann, K. Dresing, J. Breme, E. Brunner and K. M. Sturmer, *J. Biomed. Mater. Res. A*, 68 (2004) 325.
49. W. H. Lee and C. Y. Hyun, *Appl. Surf. Sci.*, 252 (2006) 4250.
50. M. Kulkarni, A. Mazare, E. Gongadze, S. Perutkova, V. Kralj-Iglic, I. Milosev, P. Schmuki, A. Iglic and M. Mozetic, *Nanotechnology*, 26 (2015) 2.
51. Y. Q. Wan, A. N. Xu, C. F. Dong, C. He, K. Xiao, Y. W. Tian and X. G. Li, *J. Mater. Sci.*, 53 (2018) 9988.
52. Y. X. Zhang, C. F. Dong, S. F. Yang, J. S. Wu, K. Xiao, Y. H. Huang and X. G. Li, *Mater. Sci. Eng. C-Mater.*, 72 (2017) 464.
53. D. Kong, C. Dong, X. Ni, L. Zhang, J. Yao, C. Man, X. Cheng, K. Xiao and X. Li, *J. Mater. Sci. Techn.*, (2019) accepted.

54. G. Pyka, G. Kerckhofs, I. Papantoniou, M. Speirs, J. Schrooten and M. Wevers, *Materials*, 6 (2013) 4737.
55. J. Vaithilingam, E. Prina, R. D. Goodridge, R. J. M. Hague, S. Edmondson, F. R. A. J. Rose and S. D. R. Christie, *Mater. Sci. Eng. C-Mater.*, 67 (2016) 294.

© 2019 The Authors. Published by ESG (www.electrochemsci.org). This article is an open access article distributed under the terms and conditions of the Creative Commons Attribution license (<http://creativecommons.org/licenses/by/4.0/>).